INTERNATIONAL JOURNAL OF ENERGY STUDIES

e-ISSN: 2717-7513 (ONLINE); homepage: https://dergipark.org.tr/en/pub/ijes

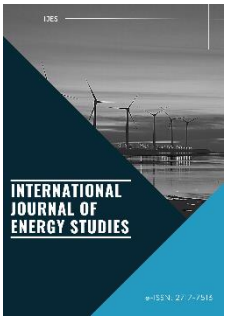

Research Article
Int J Energy Studies 2023; 8(2): 251-271
DOI: 10.58559/ijes.1295781

Received : 11 May 2023
Revised : 22 May 2023
Accepted : 01 June 2023

Comparative assessment of the various split flow supercritical CO_2 Brayton cycles for Marine gas turbine waste heat recovery

Serpil Celik Toker*
Isparta University of Applied Sciences, Department of Mechanical Engineering, Isparta, Türkiye, ORCID: 0000-0003-3572-7907
*(*Corresponding Author: serpilcelik@isparta.edu.tr)*

Highlights

- In this study, the performance of three different sCO_2 BCs for marine gas turbine waste heat recovery are compared.
- The energy efficiencies of the marine gas turbine driven TSF-1 sCO_2 BC, the TSF-2 sCO_2 BC, and the TSF-3 sCO_2 BC are calculated by 28.7%, 29.4%, and 34.5%, respectively.
- This paper provides a reference for the use of turbine split flow sCO_2 BC for marine gas turbine waste heat recovery.

You can cite this article as: Toker SC. Comparative assessment of the various split flow supercritical CO_2 Brayton cycles for Marine gas turbine waste heat recovery. Int J Energy Studies 2023; 8(2): 251-271.

ABSTRACT

Supercritical CO_2 Brayton cycle (sCO_2 BC) can become easily utilized in marine gas turbine waste heat recovery applications due to their high efficiency, compact size, and low-cost advantages. In this study, the performance of the three different split flow sCO_2 BCs, including turbine split flow-1 (TSF-1), turbine split flow-2 (TSF-2), and turbine split-3 (TSF-3), for the recovery of marine gas turbine waste heat is compared. The Engineering Equation Solver (EES) application is used to compare the three different split flow sCO_2 BCs' performances. Moreover, to investigate the influence of important thermodynamic parameters on cycle performance, a parametric analysis is carried out. The effect of variable exhaust gas temperature, turbine input pressure, and compressor inlet pressure on net power, the energy efficiency of the system, system's exergy efficiency, and exergy destruction are examined. The results suggest that the energy efficiencies of the TSF-1 sCO_2 BC, the TSF-2 sCO_2 BC, and the TSF-3 sCO_2 BC are calculated by 28.71%, 34.5%, and 29.42%, respectively. The TSF-2 sCO_2 BC has more advantages in efficiency among all the cycle layouts while the TSF-3 sCO_2 BC layout has better performance in the net power. In addition, the TSF-3 sCO_2 BC has the highest exergy destruction at 99.71 kW, followed by the TSF-1 sCO_2 BC at 91.83 kW and the TSF-2 sCO_2 BC at 41.75 kW. It has been determined that the cycle's net power increases with rising exhaust gas temperature and turbine input pressure and decreases with compressor input pressure. Exhaust gas temperature and turbine inlet pressure have a positive effect on the performance of all split flow sCO_2 BCs.

Keywords: Marine gas turbine waste heat recovery, Supercritical CO_2 Brayton cycle, Thermodynamic analysis

1. INTRODUCTION

Shipping which is around 90% of goods globally being transported, is one of the most crucial means of transport in worldwide commerce [1]. Internal combustion engines, as the principal power source for ships generally utilized [2]. These engines cause greenhouse gas effects, acid rain, and environmental pollution due to the use of poor-quality oil [3]. For this reason, the International Maritime Organization (IMO) has applied various directions since 2013 to limit pollutant emissions and increase ship energy efficiency [4-5]. The most important of these methods is waste heat recovery (WHR) technology, thanks to its great availability and the waste gas temperature of marine turbine varies between 400 °C - °600 C. [6]. Currently, technologies for marine WHR contain steam Rankine cycle [7], Brayton cycle [8], Organic Rankine cycle [9], sCO_2 BC [10], and Kalina cycle (KC). Among these cycles, the sCO_2 BC has become the focus of attention of researchers in ship WHR in recent years due to its compactness and high efficiency. CO_2 has great density and low compressibility factor thanks to the thermo-physical properties near the critical point. This significantly reduces compressor work and provides higher efficiency compared to conventional Brayton cycles [11]. This makes the sCO_2 BC stand out in the applications of marine gas turbine WHR in recent years. Sharma et al. [12] researched the energy and exergy analysis of the sCO_2 BC with regenerative and recompression for marine WHR. As a result of their investigation, they found that the addition of the sCO_2 BC to the system increased the system's energy efficiency and net power by almost 10% and 25%, respectively. Hou et al. [13] suggested an integrated system including recompression and regenerative sCO_2 BC to marine gas turbine WHR. They stated that the system's thermal efficiency increased by 12.38% when the ship was operating at full load. Pan et al. [5] focused on the multi-objective optimization and parametric study of marine gas turbine-based novel sCO_2 BC. Manjunath et al. [14] used marine gas turbine WHR for simultaneous power generation and cooling. They stated that the system's energy efficiency was raised by 11% by using the combined system consisting of sCO_2 BC and transcritical CO_2 (tCO_2) cooling system. Feng et al. [15] proposed a combined cycle comprising sCO_2 BC and KC to recover the WHR of marine engines. Uusitalo et al. [16] examined the usage of sCO_2 BCs to WHR of large-scale engines. Wang et al. [17] developed a new cascade system for engine exhaust gas WHR involving a partial heating sCO_2 BC and a tCO_2 Rankine cycle. Quyang et al. [18] suggested a new combined system for marine gas turbine applications and analyzed the system. The proposed system consists of the fuel cell, sCO_2 BC, and KC. They calculated the energy efficiency of the integrated system as 71.37%. Qin et al. [19] developed a new integrated system comprising of a marine gas turbine-driven recompression sCO_2 BC and, a

tCO_2 cooling cycle for both electricity production, and refrigeration. According to the multi-objective optimization results, the system's WHR efficiency, and COP value were calculated to be 65.1%, and 3.059, respectively. Wang et al. [20] propose a combined system for marine engine waste heat recovery. According to the multi-purpose optimization result of the proposed combined system, the energy and exergy efficiency were calculated as 33.17% and 61.93%, respectively. Sakalis [21] optimized the marine engine assisted sCO_2 BC under partial load operation. In addition, economic criteria were taken into account in determining the optimum design and operating conditions of the system

As mentioned above, there are many studies in the literature on different sCO_2 BCs for marine gas waste heat recovery. However, researches related to the thermodynamic analysis of the TSF-1, TSF-2, and TSF-3 cycles, which are from the split flow sCO_2 BC, are limited. In this context, it is aimed to assess the performance comparison of marine gas turbine-based sCO_2 BC for three different configurations, including TSF-1, TSF-2, and TSF-3. The heat required for the sCO_2 BC is provided by marine gas turbine waste heat. In order to examine the impacts of the key process parameters on the system performance, parametric studies are conducted according to the exhaust gas temperature, the compressor, and turbine input pressure.

2. SYSTEM CONFIGURATIONS

Figure 1 displays the schematic configurations of the TSF-1 sCO_2 BC (a), TSF-2 sCO_2 BC (b), and TSF-3 sCO_2 BC (c), respectively. All three cycles consist of a gas cooler, compressor, low temperature recuperator (LTR), high temperature recuperator (HTR), turbine-1, turbine-2, and heater. Although the equipment types and numbers in all three cycles are the same, the ways of completing the cycle of the divided fluids are different. In the TSF-1 sCO_2 BC, some portion of the fluid in the compressor outlet is passed through the HTR, and work is produced in the turbine. Another part of the agent leaving the compressor is passed through the LTR and sent to the heater. The agent coming from the evaporator is sent to the gas cooler via HTR by generating work in the turbine. In the TSF-2 sCO_2 BC, some portion of the working agent in the compressor outlet first enters the LTR and then the turbine, producing work, while the other leaving fluid first enters the HTR and then the heater. Finally, some amount of the fluid separated at the compressor outlet is passed through LTR and HTR before being sent to turbine-1 in the TSF-3 sCO_2 BC. Another part of the fluid separated at the compressor outlet is sent directly to the heater without being subjected

to any preheating. Figure 2 demonstrates the T-s diagrams of the TSF-1 sCO_2 BC (a), the TSF-2 sCO_2 BC (b), and the TSF-3 sCO_2 BC (c), respectively.

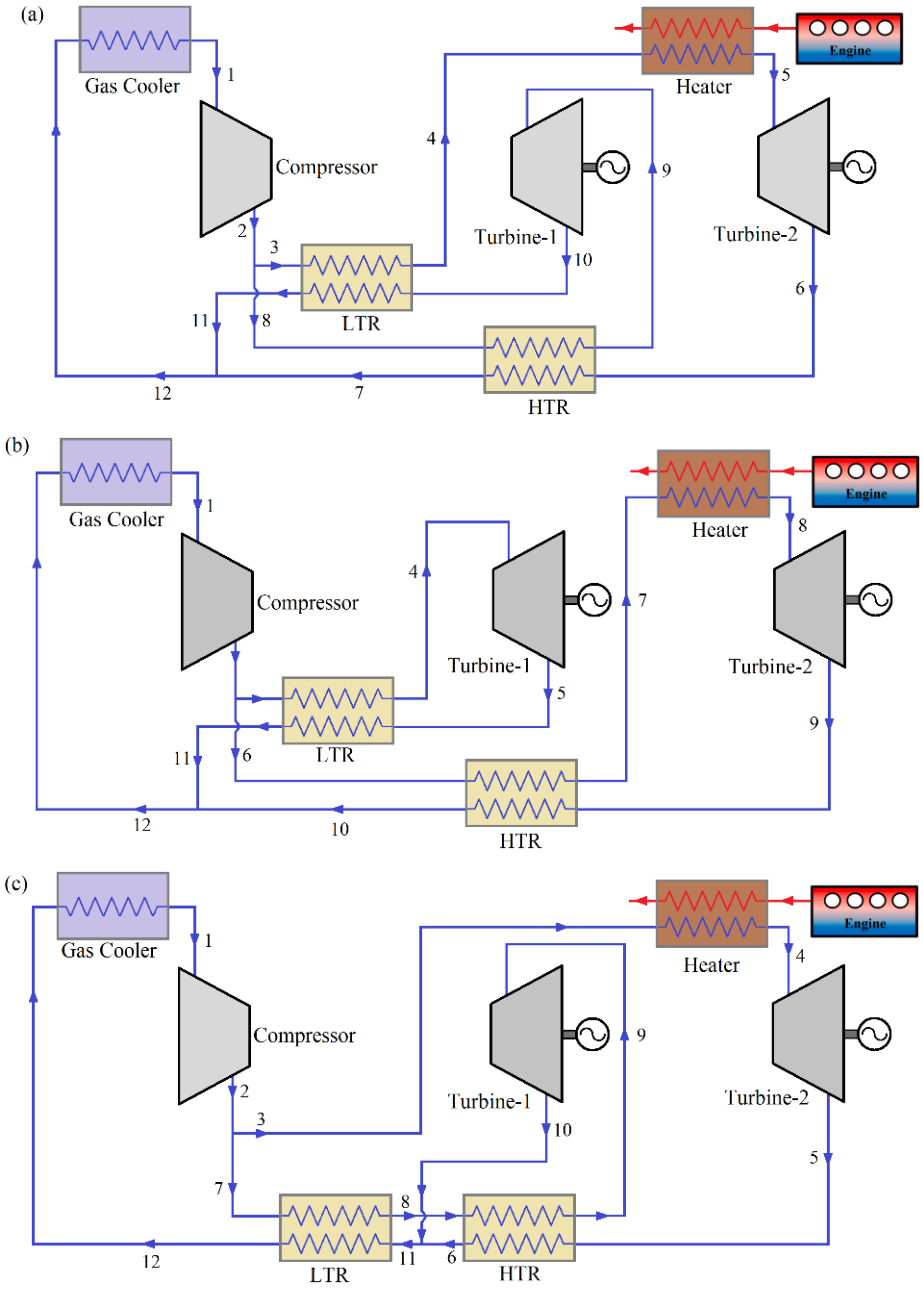

Figure 1. Configurations of the TSF-1 sCO_2 BC (a), TSF-2 sCO_2 BC (b), and TSF-3 sCO_2 BC (c)

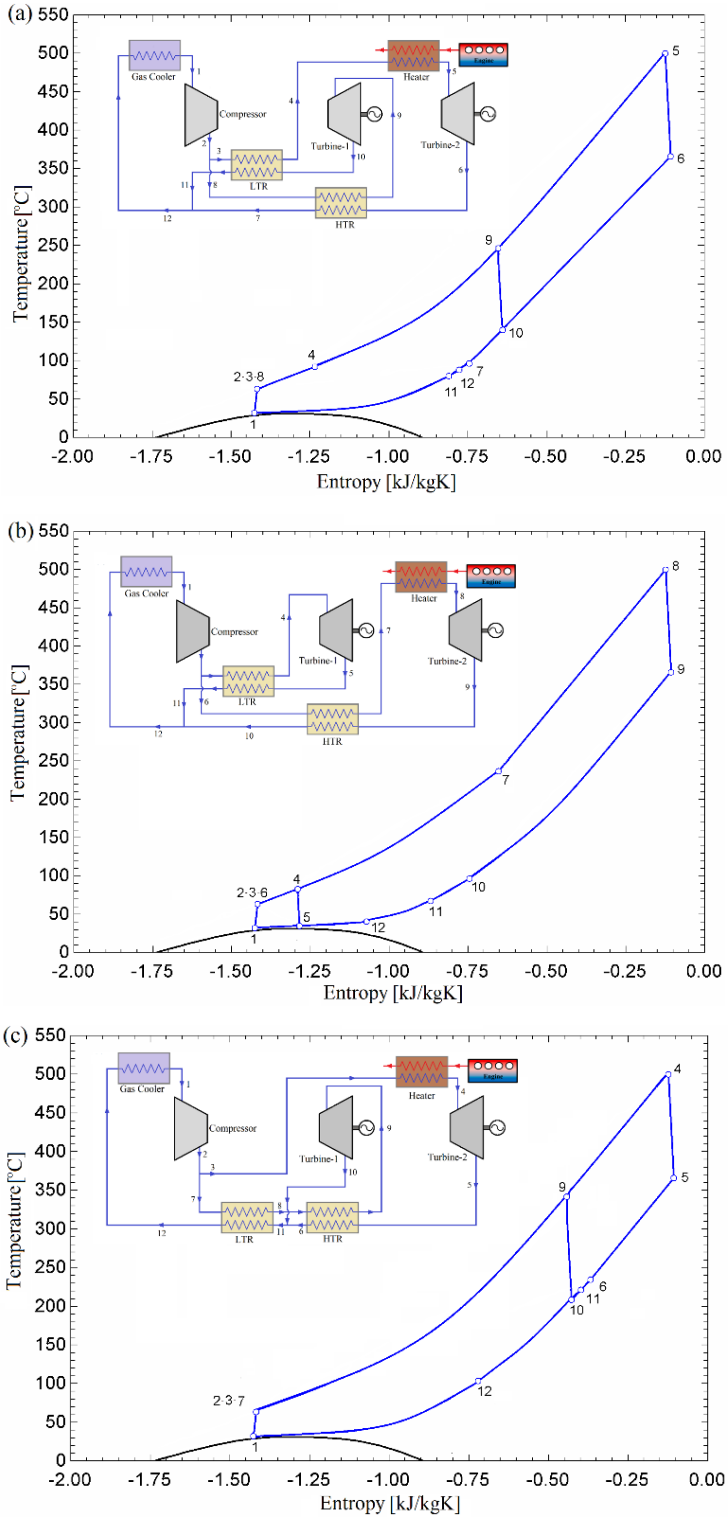

Figure 2. T-s diagrams of the sCO_2 BC TSF-1 (a), TSF-1 sCO_2 BC (b), and TSF-1 sCO_2 BC (c)

3. THERMODYNAMIC ANALYSIS

The performances of the three various split flow sCO_2 BCs are compared utilizing the EES program. The following presumptions are used to make the thermodynamic analysis more straightforward [22, 23]:

- It is assumed that all cycle is operating in a steady-state condition.
- Pressure variations, kinetic, and potential energies are disregarded.
- It is accepted that CO_2 is a saturated liquid at the condenser output.
- The reference state for the cycles has an environmental temperature of T_0=25 °C and a pressure of P_0=101.325 kPa.

The steady-state mass balance equation is expressed as [24]:

$$\sum \dot{m}_{in} = \sum \dot{m}_{out} \tag{1}$$

where, $\dot{m}$ is the mass current, and subscripts "in" and "out" are the input and output conditions. According to Dincer and Rosen [24], the energy equilibrium for the exergy analysis is as follows:

$$\sum \dot{m}_{in} h_{in} + \sum \dot{Q}_{in} + \sum \dot{W}_{in} = \sum \dot{m}_{out} h_{out} + \sum \dot{Q}_{out} + \sum \dot{W}_{out} \tag{2}$$

Here, h is the specific enthalpy, $\dot{Q}$ is the rate of heat, and $\dot{W}$ is the rate of work. For the exergy analysis, the exergy equilibrium is determined as [20]:

$$\begin{aligned} \sum \dot{m}_{in} ex_{flow} + \sum \dot{E}x_{in}^{Q} + \sum \dot{E}x_{in}^{W} \\ = \sum \dot{m}_{out} ex_{flow} + \sum \dot{E}x_{out}^{Q} + \sum \dot{E}x_{out}^{W} + \dot{E}x_{dest} \end{aligned} \tag{3}$$

where, ex_{flow} is the agent's exergy, and $\dot{E}x_{dest}$ is the exergy irreversibility.

The compressor's and turbine's isentropic efficiencies in the TSF-1 sCO_2 BC are determined as follows:

$$\eta_{is,C} = \frac{h_{2s} - h_1}{h_{2a} - h_1} \quad (4)$$

$$\eta_{is,T-1} = \frac{h_9 - h_{10a}}{h_9 - h_{10s}} \quad (5)$$

The subscripts "a" and "s" in the above equation denote the enthalpy in the real and isentropic states, respectively.

The effectiveness of LTR and HTR in the TSF-1 sCO_2 BC are calculated using the relations defined below [25]:

$$\varepsilon_{LTR} = \frac{h_{10} - h_{11}}{h_{10} - h_3(T_3, P_{11})} \quad (6)$$

$$\varepsilon_{HTR} = \frac{h_6 - h_7}{h_6 - h_{8rec}(T_8, P_7)} \quad (7)$$

In split flow sCO_2 BCs, the flow is split into two in a certain part of the cycle. The split ratio (SR) presents the rate of the 3-state mass flow to the 2-state mass flow and is given by

$$SR = \dot{m}_3/\dot{m}_2 \quad (8)$$

As for the three sCO_2 BCs, the energy, and exergy efficiencies are described as follows:

$$\eta_{en} = \frac{\dot{W}_{net}}{\dot{Q}_{in}} \quad (9)$$

$$\eta_{ex} = \frac{\dot{W}_{net}}{\dot{E}x_{Q_{in}}} \quad (10)$$

Here, $\dot{W}_{net}$ denotes the cycle's net power, $\dot{Q}_{in}$ represents the heat entering the cycle, and $\dot{E}x_{Q_{in}}$ indicates the exergy of the heat. The main design parameters of the sCO_2 BCs are listed in Table 1.

Table 1. Design parameters of the sCO_2 BC

Parameters	Value
Exhaust gas temperature	550 °C
Pinch point temperature difference in heater	50 °C
Compressor input temperature	32 °C [22]
Turbine input pressure	25000 kPa [22]
Pressure ratio	3.125
Turbine's isentropic efficiency	0.93 [26]
Compressor's isentropic efficiency	0.89 [22]
HTR effectiveness	0.85 [27]
LTR effectiveness	0.70 [27]
Split ratio	0.50

4. RESULTS AND DISCUSSIONS

In this paper, the exergy and energy performances of three various sCO_2 BC are investigated using EES software [28]. Moreover, a parametric study was performed to examine the impacts of exhaust gas temperature, turbine input pressure, and compressor input pressure on cycle performance. Thermodynamic analysis of the TSF-1 sCO_2 BC, TSF-2 sCO_2 BC, and TSF-3 sCO_2 BC is performed according to the main design parameters, and thermophysical properties like pressure, temperature, mass flow rate, enthalpy, and entropy of each point forming the cycle are given in Table 2.

Figure 3 (a), and (b) provides the comparison of the examined marine gas turbine based sCO_2 BCs in terms of net power, exergy destruction, energy, and exergy efficiency. The TSF-2 sCO_2 BC can yield the most excellent performances, and followed by the TSF-2 sCO_2 BC, while the TSF-1 sCO_2 BC yields the worst performances. TSF-3 sCO_2 BC showed the highest net power work value as compared to TSF-1 sCO_2 BC , and TSF-2 sCO_2 BC. Considering the exergy destruction, the highest exergy destruction was calculated for the TSF-3 sCO_2 BC, and the lowest exergy destruction was founded for the TSF-2 sCO_2 BC.

Table 2. Thermodynamic properties of each point in the sCO_2 BC

Cycle	State	T [°C]	P [kPa]	h [kJ/kg]	s [kJ/kgK]	ṁ [kg/s]	ex [kJ/kg]	**Ėx** [kW]
Turbine Split Flow-1	1	32.00	8000	-210.4	-1.426	1.0	215.2	215.2
	2	63.53	25000	-184.0	-1.418	1.0	239.0	239.0
	3	63.53	25000	-184.0	-1.418	0.5	239.0	119.5
	4	92.22	25000	-119.7	-1.234	0.5	248.7	124.3
	5	500.0	25000	462.4	-0.1242	0.5	499.8	249.9
	6	365.9	8000	321.2	-0.1075	0.5	353.5	176.8
	7	96.79	8000	8.797	-0.7454	0.5	231.3	115.7
	8	63.53	25000	-184.0	-1.418	0.5	239.0	119.5
	9	237.0	25000	128.4	-0.6537	0.5	323.6	161.8
	10	128.9	8000	49.83	-0.6389	0.5	240.6	120.3
	11	80.40	8000	-14.49	-0.8098	0.5	227.2	113.6
	12	88.39	8000	-2.848	-0.7772	1.0	229.2	229.2
Turbine Split Flow-2	1	32.00	8000	-210.4	-1.426	1.0	215.2	215.2
	2	63.53	25000	-184.0	-1.418	1.0	239.0	239.0
	3	63.53	25000	-184.0	-1.418	0.5	239.0	119.5
	4	83.08	25000	-140.3	-1.291	0.5	245.1	122.5
	5	34.63	8000	-167.0	-1.285	0.5	216.4	108.2
	6	63.53	25000	-184.0	-1.418	0.5	239.0	119.5
	7	237.0	25000	128.4	-0.6537	0.5	323.6	161.8
	8	500.0	25000	462.4	-0.1242	0.5	499.8	249.9
	9	365.9	8000	321.2	-0.1075	0.5	353.5	176.8
	10	96.79	8000	8.797	-0.7454	0.5	231.3	115.7
	11	67.58	8000	-34.94	-0.8687	0.5	224.4	112.2
	12	40.62	8000	-100.9	-1.072	1.0	218.9	218.9
Turbine Split Flow-3	1	32.00	8000	-210.4	-1.426	1.0	-1.426	215.2
	2	63.53	25000	-184.0	-1.418	1.0	-1.418	239.0
	3	63.53	25000	-184.0	-1.418	0.5	-0.709	239.0
	4	500.0	25000	462.4	-0.1242	0.5	-0.062	499.8
	5	365.9	8000	321.2	-0.1075	0.5	-0.054	353.5
	6	234.7	8000	172.2	-0.3684	0.5	-0.184	282.3
	7	63.53	25000	-184.0	-1.418	0.5	-0.709	239.0
	8	213.3	25000	95.25	-0.7203	0.5	-0.360	310.3
	9	325.6	8000	244.3	-0.4441	0.5	-0.222	377.0
	10	208.6	8000	142.6	-0.4281	0.5	-0.214	270.6
	11	221.6	8000	157.4	-0.3979	1.0	-0.398	276.3
	12	103.5	8000	17.78	-0.7213	1.0	-0.721	233.1

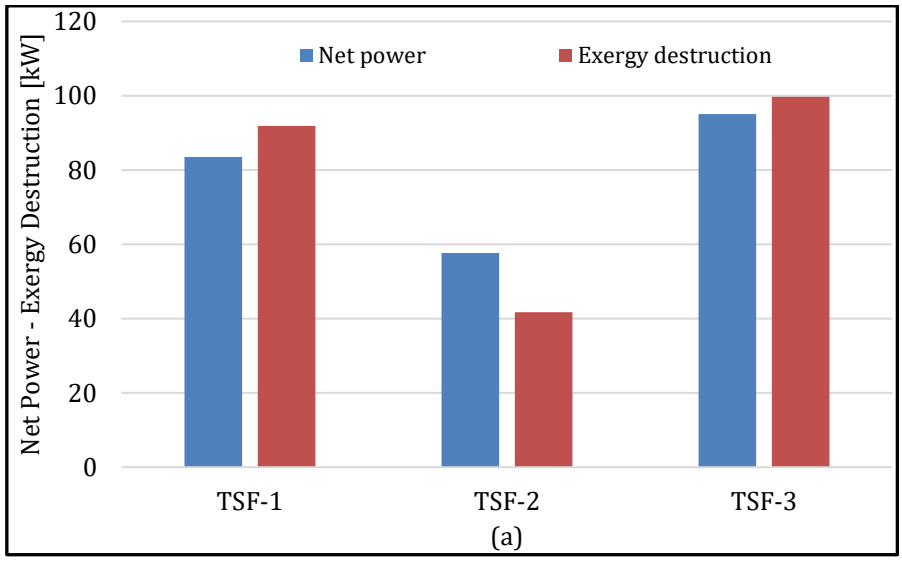

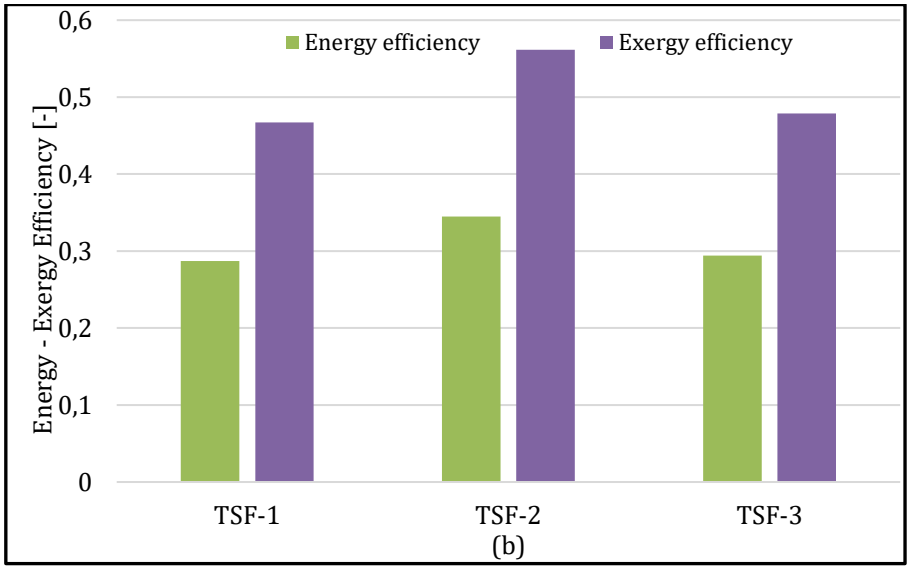

Figure 3. Net power- exergy destruction (a), Energy- exergy efficiency (b) of the various sCO_2 BCs

Figure 4 displays the waste gas exhaust temperature impact on the system's net power. It can be seen that the net power of the three sCO_2 BCs is raised with the up of the exhaust waste gas temperature. As the exhaust gas temperature increases, the net power of the TSF-3 sCO_2 BC rises from 68.0 kW to 129.3 kW, while the net power of the TSF-2 sCO_2 BC increases from 45.8 kW to 74.63 kW.

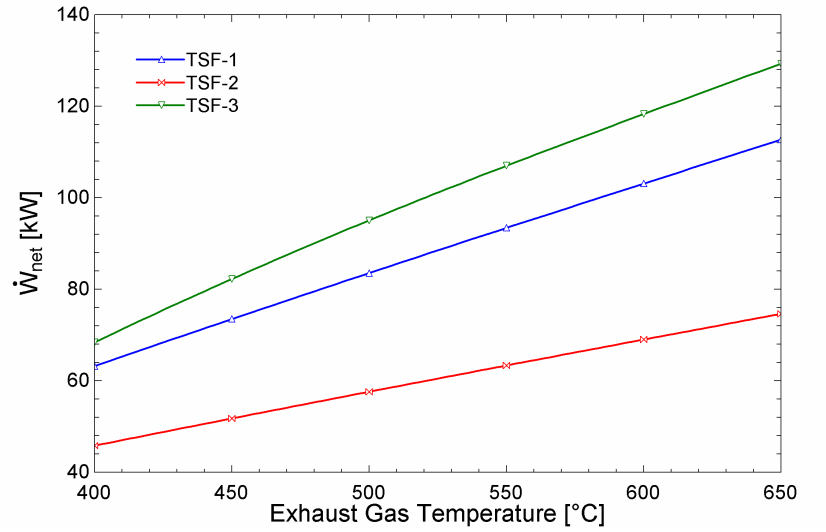

Figure 4. Impact of exhaust gas temperature on net power

Figure 5 illustrates the variation of the examined sCO_2 BC's energy efficiency with the exhaust gas temperature. As can be seen from the figure, with the increase of exhaust gas temperature, energy efficiency values rise for all cycles. The highest energy efficiency is in the TSF-2 sCO_2 BC. Although the net power produced in the TSF-2 sCO_2 BC is the lowest, the reason for the high energy efficiency is the low heat energy entering the cycle.

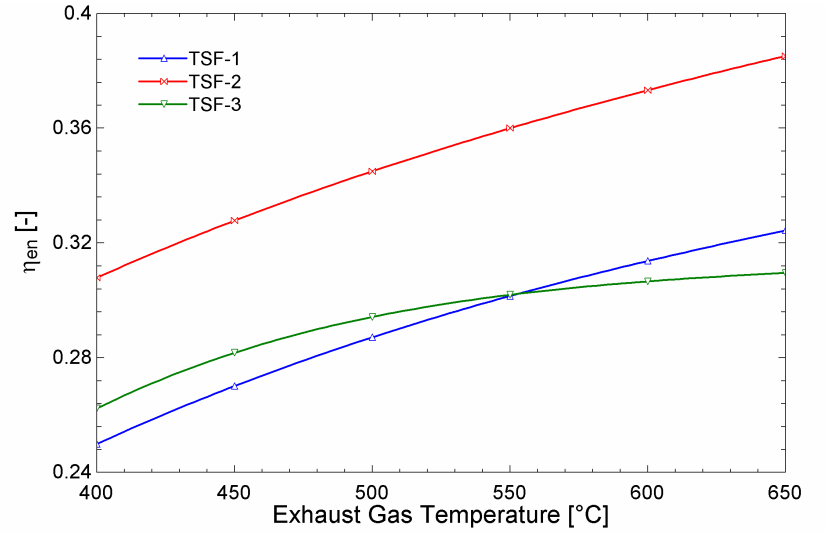

Figure 5. Effect of exhaust gas temperature on energy efficiency

Figure 6 reflects the impacts of exhaust gas temperature on the system's exergy irreversibility. It can be observed that exergy destruction of all turbine split flow sCO_2 BC rises with the waste gas temperature's increment. The highest exergy destruction was founded for the TSF-3 sCO_2 BC, and

the lowest exergy destruction was calculated for the TSF-2 sCO_2 BC. At the same time, the gas temperature increased from 400 °C to 650 °C, exergy destruction raised by 60%, 58%, and 101%, respectively, in the TSF-1 sCO_2 BC, TSF-2 sCO_2 BC, and TSF-3 sCO_2 BC.

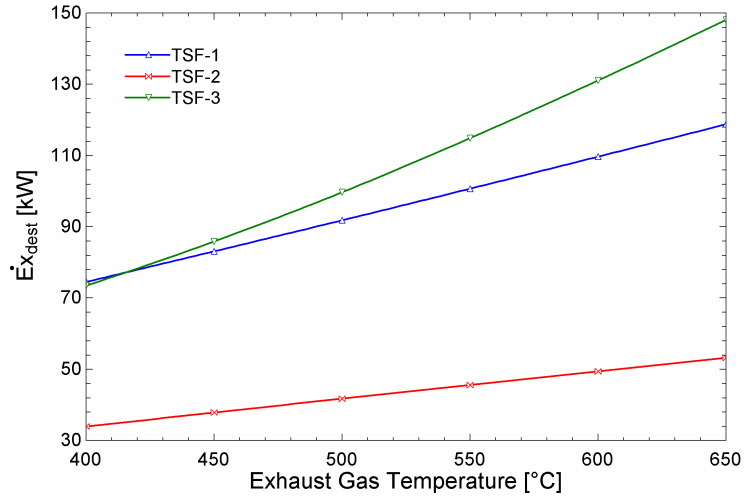

Figure 6. Impact of exhaust gas temperature on exergy destruction

Finally, the impact of exhaust gas temperature on cycle exergy efficiency is demonstrated in Figure 7. While the exergy efficiency of the TSF-1 sCO_2 BC and the turbine split flow-2 sCO_2 BC increases with the exhaust gas temperature, the exergy destruction of the TSF-3 sCO_2 BC first increases with increasing gas temperature, and then there is a slight decrease. The reason for the decrease in exergy efficiency in the TSF-3 sCO_2 BC is that the inlet heat exergy increases more than the net power.

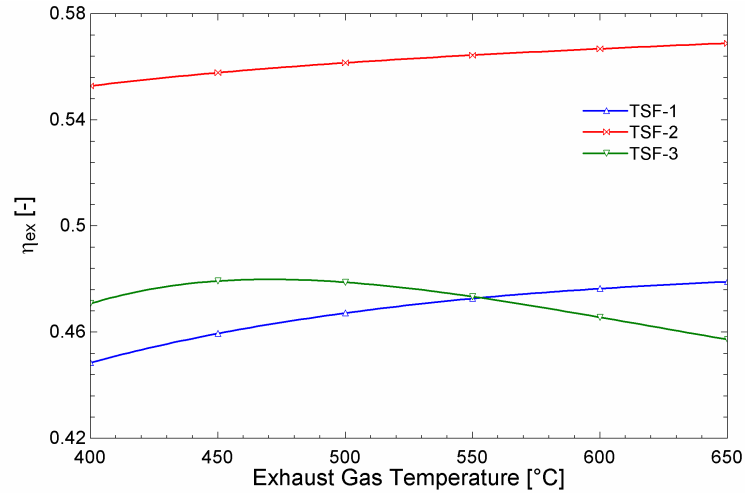

Figure 7. Impact of exhaust gas temperature on exergy efficiency

The impact of turbine inlet pressure has been examined for the three sCO_2 BC for net power with a turbine input temperature of 550 °C. Figure 8 exhibits the changing trend of the cycle's net power with the turbine inlet pressure. For any given compressor input pressure value, it can be observed that the lowest net power is calculated by the TSF-2 sCO_2 BC, as shown in Figure 8, and the highest net power is founded by the TSF-3 sCO_2 BC.

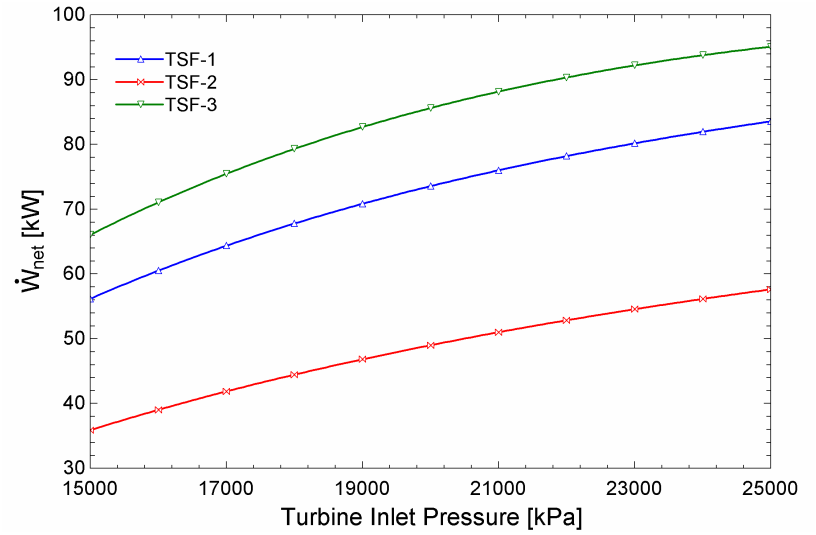

Figure 8. Impact of turbine inlet pressure on net power

The result of the effect of turbine inlet pressure on energy efficiency is presented in Figure 9. The energy efficiency of all sCO_2 BCs increased as the turbine input pressure increased from 15000 kPa to 25000 kPa. In case the turbine input pressure is 20500 kPa, the energy efficiency from the highest to the lowest is the TSF-2 sCO_2 BC, the TSF-3 sCO_2 BC, and the TSF-1 sCO_2 BC. For the three different configurations examined, energy efficiency raised by 29%, 49%, and 31%, respectively.

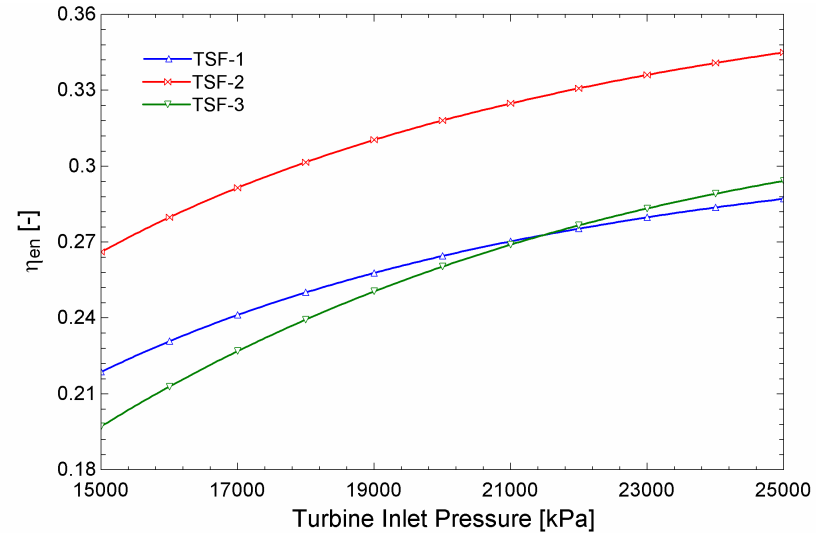

Figure 9. Impact of turbine inlet pressure on energy efficiency

The behavior of exergy irreversibility with rising turbine inlet pressure is illustrated in Figure 10. As can be seen from the graph, as the turbine inlet pressure increases, the exergy destruction of the sCO_2 BC also reduces. The reason for the reduction in the exergy destruction rate is that the turbine work increases with rising turbine inlet pressure, and the increment in turbine power leads to a reduction in the exergy destruction rate for the turbine. With turbine input pressure, the exergy irreversibility ratio decreases sharply for TSF-1 sCO_2 BC, while the decrease in exergy irreversibility ratio for TSF-1 sCO_2 BC and TSF-2 sCO_2 BC reduces slowly.

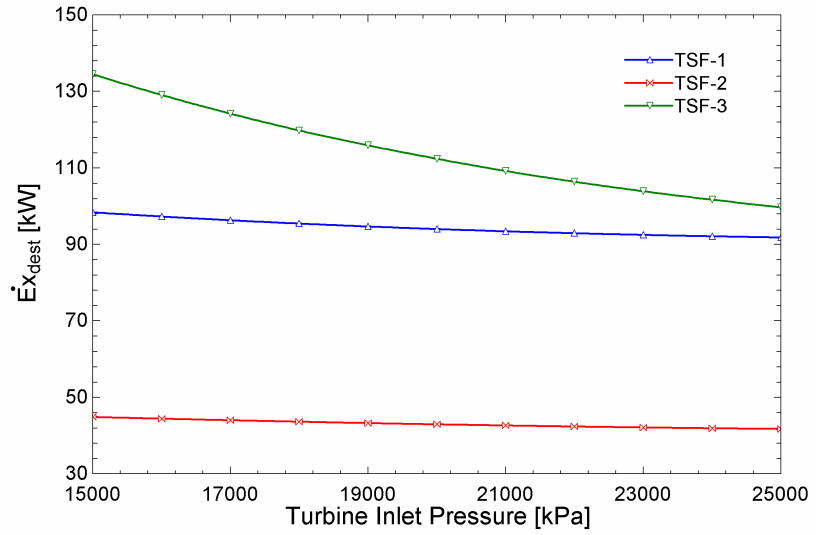

Figure 10. Impact of turbine inlet pressure on exergy destruction

Exergy analysis of the cycle layouts evaluated in this paper is shown in Figure 11. The findings imply that exergy efficiency rises with the enhancement in the turbine inlet pressure for cycle layouts considerably. With the increase in turbine input pressure, the exergy efficiency of the TSF-1 sCO_2 BC rises to 46.7 % at 35.6%, the efficiency of the TSF-2 sCO_2 BC expands to 56.2% at 43.3%, and the efficiency of the TSF-3 sCO_2 BC improves to 47.8% at 32.1%.

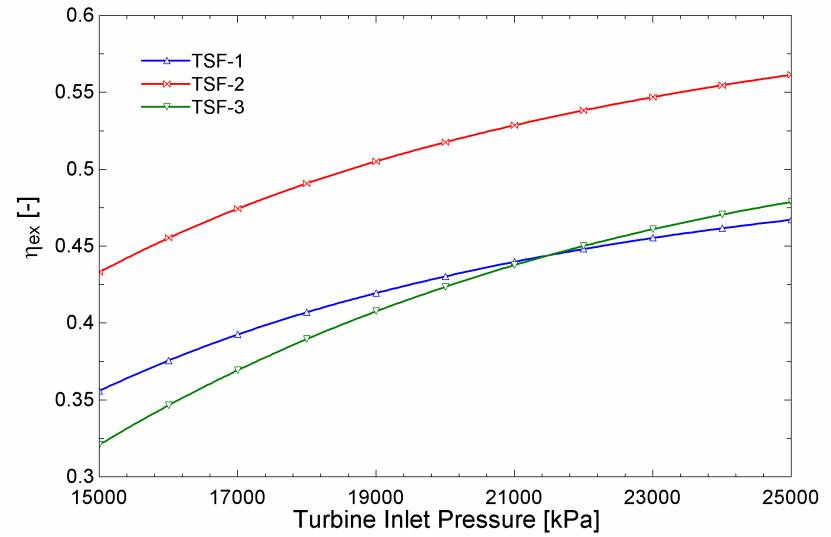

Figure 11. Effect of turbine inlet pressure on exergy efficiency

Figure 12 illustrates how the cycle's net power changes as the compressor input pressure rises. With the rise of the compressor input pressure, the system's net power reduces significantly. As the cycle's net power decreases with the rise of the compressor inlet pressure, the net power value of all the cycles has diminished. 50% pressure increase in compressor inlet pressure causes 22%, 32%, and 21% decrease in net power amount in the TSF-1 sCO_2 BC, the TSF-2 sCO_2 BC, and the TSF-3 sCO_2 BC, respectively.

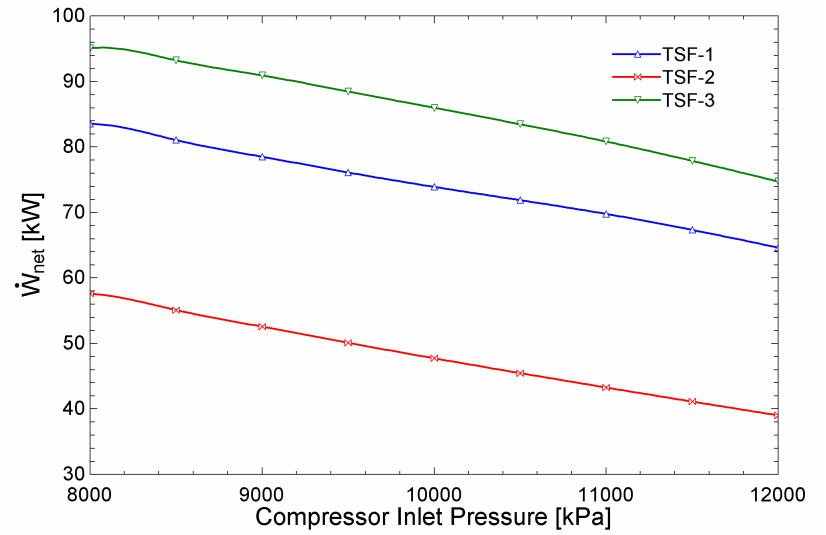

Figure 12. Impact of compressor inlet pressure on net power

The cycle's energy efficiency for a range of compressor inlet pressure is displayed in Figure 13. As shown in the figure, variable compressor input pressure has a different impact on the cycles considered. While the tendency of the TSF-1 sCO_2 BC and the TSF-2 sCO_2 BC to change according to the changing compressor pressure is the same, it is different in the TSF-3 sCO_2 BC. The energy efficiency for the TSF-1 sCO_2 BC and the TSF-2 sCO_2 BC reaches their minimum values when the compressor input pressure is 9600 kPa.

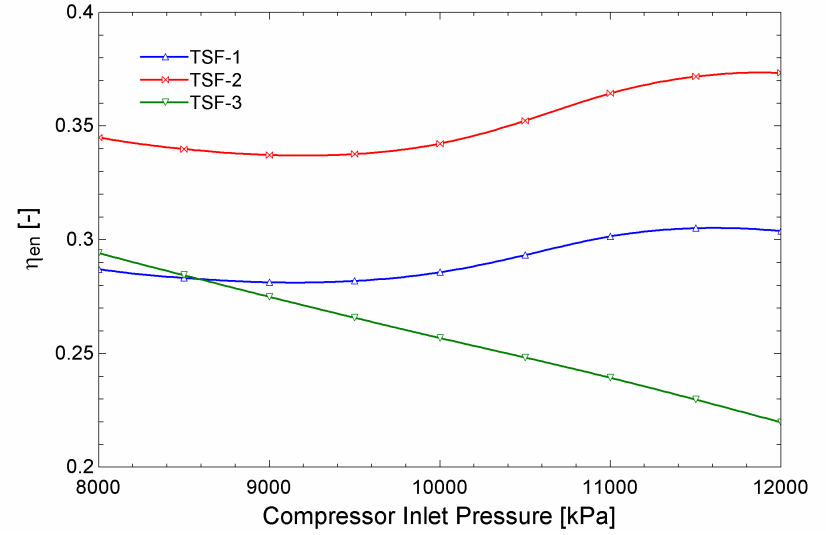

Figure 13. Effect of compressor inlet pressure on energy efficiency

Figure 14 exhibits the comparison of the energy efficiency of three different sCO_2 BCs at various compressor inlet pressure. It can be seen that, except for the TSF-3 sCO_2 BC, the energy efficiency

reduces with the rise in compressor inlet pressure. Figure 15 demonstrates the results of the altered compressor inlet pressure on the cycle's energy efficiency. It can be seen that the TSF-1 sCO_2 BC and the TSF-2 sCO_2 BC showed an almost parallel trend with rising pressure values.

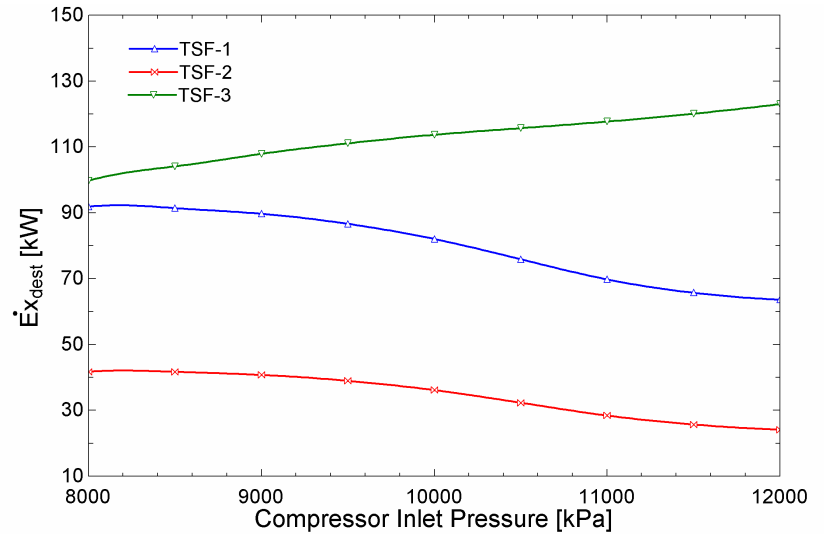

Figure 14. Effect of compressor inlet pressure on exergy destruction

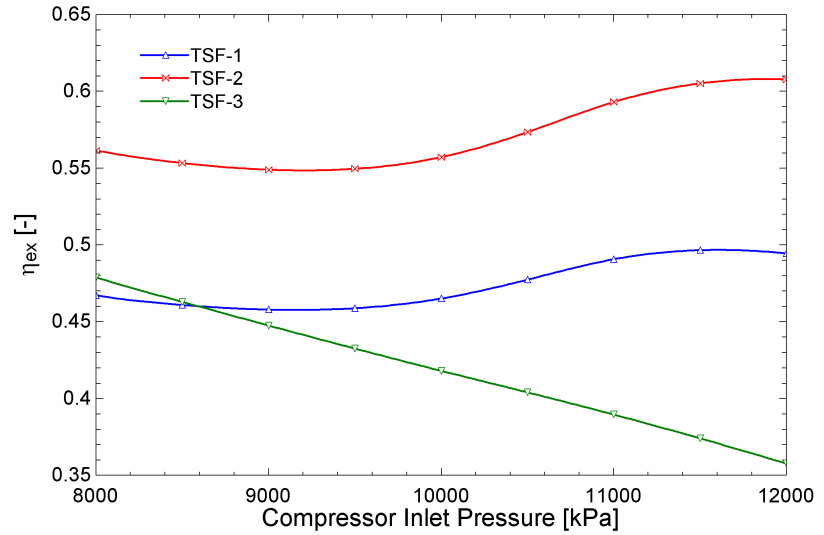

Figure 15. Effect of compressor inlet pressure on exergy efficiency

5. CONCLUSION

In this paper, a comparative analysis was performed for the performances of three various sCO_2 BCs (TSF-1, TSF-2, TSF-3) for marine gas turbine waste heat recovery. The mathematical modeling of the studied three different turbine split flow sCO_2 BC was established using the EES program. The key thermodynamic parameters used to evaluate the performance of the sCO_2 BCs

are exhaust gas temperature, turbine inlet pressure, and compressor inlet pressure. The key outcomes drawn from the paper are summarized as follows:

- The energy efficiencies of the TSF-1 sCO_2 BC, the TSF-2 sCO_2 BC, and the TSF-3 sCO_2 BC are calculated by 28.7%, 29.4%, and 34.5%, respectively, under design parameters.

- The highest net power work value was calculated in the TSF-3 sCO_2 BC when compared to TSF-1 sCO_2 BC and TSF-2 sCO_2 BC.

- According to calculations of exergy destruction, the TSF-3 sCO_2 BC had the highest exergy destruction while the TSF-2 sCO_2 BC had the lowest exergy destruction.

- When the exhaust gas temperature increases from 450 °C to 650 °C, the net power of the TSF-3 sCO_2 BC rises from 68.0 kW to 129.3 kW, while the net power of the TSF-2 sCO_2 BC increases from 45.8 kW to 74.63 kW.

- It is found that the net power of the cycle increases with turbine inlet pressure and decreases with compressor inlet pressure.

- Lastly, this paper ensures a reference for searchers to examine the usage of turbine split flow sCO_2 BC to recycle the marine gas turbine waste heat.

NOMENCLATURE

BC Brayton cycle
HTR High temperature recuperator
KC Kalina cycle
LTR Low temperature recuperator
sCO2 Supercritical carbon dioxide
tCO2 Transcritical carbon dioxide
TSF-1 Turbine split flow-1
TSF-2 Turbine split flow-2
TSF-3 Turbine split flow-3
WHR Waste heat recovery

DECLARATION OF ETHICAL STANDARDS

The author of the paper submitted declares that nothing which is necessary for achieving the paper requires ethical committee and/or legal-special permissions.

CONTRIBUTION OF THE AUTHORS

Serpil Celik Toker: Wrote the manuscript.

CONFLICT OF INTEREST

There is no conflict of interest in this study.

REFERENCES

[1] Poulsen RT, Johnson H. The logic of business vs. the logic of energy management practice: understanding the choices and effects of energy consumption monitoring systems in shipping companies. Journal of Cleaner Production 2016; 112: 3785-3797.

[2] Alagumalai A. Internal combustion engines: Progress and prospects. Renewable and Sustainable Energy Reviews 2014; 38: 561-571.

[3] Jiaqiang E, Zhang Z, Chen J. Pham M, Zhao X, Peng Q, Zhang B, Yin Z. Performance and emission evaluation of a marine diesel engine fueled by water biodiesel-diesel emulsion blends with a fuel additive of a cerium oxide nanoparticle. Energy Conversion and Management 2018; 169: 194-205.

[4] MAN Diesel & Turbo. 8S90ME-C10.5 with high load tuning. CEAS Engine Data Report.

[5] Pan P, Yuan C, Sun Y, Yan X, Lu M, Bucknall R. Thermo-economic analysis and multi-objective optimization of S-CO_2 Brayton cycle waste heat recovery system for an ocean-going 9000 TEU container ship. Energy Conversion and Management 2020; 221: 113077.

[6] Zhu S, Zhang K, Deng K. A review of waste heat recovery from the marine engine with highly efficient bottoming power Cycles. Renewable and Sustainable Energy Reviews 2020; 120: 109611.

[7] Larsen U, Sigthorsson O, Haglind F. A comparison of advanced heat recovery power cycles in a combined cycle for large ships. Energy 2014; 74: 260-268.

[8] Yang Y, Huang Y, Jiang P, Zhu Y. Multi-objective optimization of combined cooling, heating, and power systems with supercritical CO_2 recompression Brayton cycle. Applied Energy 2020; 271: 115189.

[9] Han F, Wang Z, Ji Y, Li W, Sundén B. Energy analysis and multi-objective optimization of waste heat and cold energy recovery process in LNG-fueled vessels based on a triple organic Rankine cycle. Energy Conversion and Management 2019; 195: 561-572.

[10] Ouyang T, Wang Z, Wang G, Zhao Z, Xie S, and Li X. Advanced thermo-economic scheme and multi-objective optimization for exploiting the waste heat potentiality of marine natural gas engine. Energy 2021; 236: 121440.

[11] Cha JE, Park JH, Lee G, Seo H, Lee S, Chung HJ, Lee SW. 500 kW supercritical CO_2 power generation system for waste heat recovery: System design and compressor performance test results. Applied Thermal Engineerinhg 2021; 194: 117028.

[12] Sharma OP, Kaushik SC, Manjunath K. Thermodynamic analysis and optimization of a supercritical CO_2 regenerative recompression Brayton cycle coupled with a marine gas turbine for shipboard waste heat recovery. Thermal Science and Engineering Progress 2017; 3: 62-74.

[13] Hou S, Wu Y, Zhou Y, Yu L. Performance analysis of the combined supercritical CO_2 recompression and regenerative cycle used in waste heat recovery of marine gas türbine. Energy Conversion and Management 2017; 151: 73-85.

[14] Manjunath K, Sharma OP, Tyagi SK, Kaushik SC. Thermodynamic analysis of a supercritical/transcritical CO_2 based waste heat recovery cycle for shipboard power and cooling applications. Energy Conversion and Management 2018; 155: 262-275.

[15] Feng Y, Du Z, Shreka M, Zhu Y, Zhou S, Zhang W. Thermodynamic analysis and performance optimization of the supercritical carbon dioxide Brayton cycle combined with the Kalina cycle for waste heat recovery from a marine low-speed diesel engine. Energy Conversion and Management 2020; 206: 112483.

[16] Uusitalo A, Ameli A, Turunen-Saaresti T. Thermodynamic and turbomachinery design analysis of supercritical Brayton cycles for exhaust gas heat recovery. Energy 20019; 167: 60-79.

[17] Wang Z, Jiang Y, Ma Y, Han F, Ji Y, Cai W. A partial heating supercritical CO_2 nested transcritical CO_2 cascade power cycle for marine engine waste heat recovery: Thermodynamic, economic, and footprint analysis. Energy 2022; 261: 125269.

[18] Ouyang T, Zhao Z, Su Z, Lu J, Wang Z, Huang H. An integrated solution to harvest the waste heat from a large marine solid oxide fuel cell. Energy Conversion and Management 2020; 223: 133318.

[19] Qin L, Xie G, Ma Y, Li S. Thermodynamic analysis and multi-objective optimization of a waste heat recovery system with a combined supercritical/transcritical CO_2 cycle. Energy 2023; 265: 126332.

[20] Wang Z, Jiang Y, Han F, Yu S, Li W, Ji Y, Cai W. A thermodynamic configuration method of combined supercritical CO_2 power system for marine engine waste heat recovery based on recuperative effects . Applied Thermal Engineering 2022; 200: 117645.

[21] Sakalis G.N. Design and partial load operation optimization of integrated ship Energy system based on supercritical CO_2 waste heat recovery cycle. Sustainable Energy Technologies and Assessments 2022; 51: 101965.

[22] Khatoon S, Kim MH. Potential improvement and comparative assessment of supercritical Brayton cycles for arid climate. Energy Conversion and Management 2019; 200: 112082.

[23] Akbari A.D, Mahmoudi S.M.S. Thermoeconomic analysis & optimization of the combined supercritical CO_2 (carbon dioxide) recompression Brayton/organic Rankine cycle. Energy 2014; 78: 501-512.

[24] Dincer I, Rosen MA. Exergy and energy analyses. Exergy 2013; 21-30.

[25] Chen K, Qin J, Sun H, Li H, He S, Zhang S, Bao W. Power optimization and comparison between simple recuperated and recompressing supercritical carbon dioxide Closed-Brayton-Cycle with finite cold source on hypersonic vehicles. Energy 2019; 181: 1189-1201.

[26] Wang K, Li MJ, Guo JQ, Li P, Liu ZB. A systematic comparison of different S-CO_2 Brayton cycle layouts based on multi-objective optimization for applications in solar power tower plants. Applied Energy 2018; 212: 109-121.

[27] Al-Sulaiman FA, Atif M. Performance comparison of different supercritical carbon dioxide Brayton cycles integrated with a solar power tower. Energy 2015; 82: 61-71.

[28] K. Sanford, Engineering equation solver (EES), 2023.